

Electronic Supplementary Information for

Plasmonic color metasurfaces fabricated by a high speed roll-to-roll method

Swathi Murthy¹, Henrik Pranov², Nikolaj A. Feidenhans'1^{3,4}, Jonas S. Madsen³, Poul Erik Hansen³, Henrik C. Pedersen¹, and Rafael Taboryski^{4,*}

¹ Department of Photonics Engineering, Technical University of Denmark, Frederiksborgvej 399, DK-4000 Roskilde, Denmark

² Heliac ApS, Ambolten 8, DK-2970 Hørsholm, Denmark

³ Danish Fundamental Metrology A/S, Matematiktorvet 307, DK-2800 Kgs. Lyngby, Denmark

⁴ Department of Micro- and Nanotechnology, Technical University of Denmark, DK-2800 Kgs. Lyngby, Denmark

*rata@nanotech.dtu.dk

Contents

S1. Extrusion coating – principle of operation.....	2
S2. Effect of encapsulation	3
S3. Comparison between constant versus varying gap configuration.....	4
S4. Comparison of simulation spectra with sharp and rounded edges	4
S5. Coupling between pillar and cavity plasmons	5
S6. Diameter and depth variation at constant pitch and metal thickness.....	6
S7. Measured and simulated spectra for 20 nm samples.....	7
S8. Comparison of R2R and batch metalized samples.....	8
S9. R2R metallization – principle of operation	9
S10. LED lamp spectrum	9

S1. Extrusion coating – principle of operation

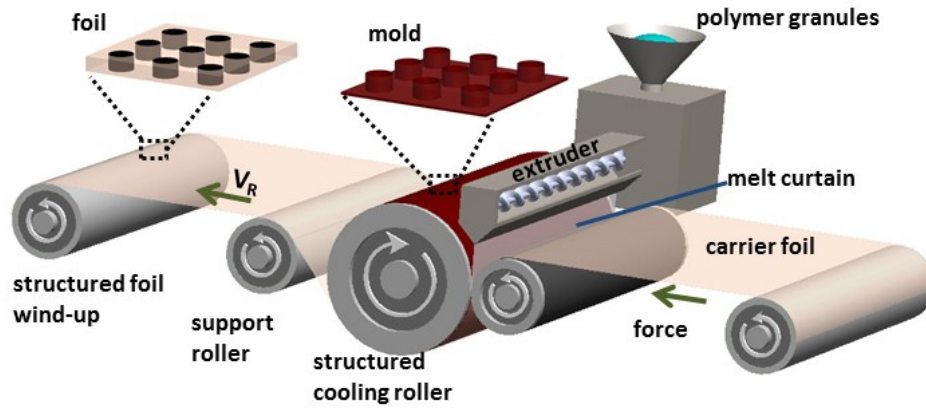


Figure S1. 3D drawing of roll-to-roll extrusion coating. A polymer melt curtain is extruded through a flat die, before being laminated onto a carrier foil. The lamination occurs as the melt curtain is pressed between a structured cooling roll (maintained at a temperature below the solidification temperature of the polymer by running water through it) and the pressure roll made of silicone rubber wrapped around a metal core. The relief structure from the structured cooling roll is replicated into the thermoplastic film before it solidifies. The structured foil is finally wound up onto the winding roll.

S2. Effect of encapsulation

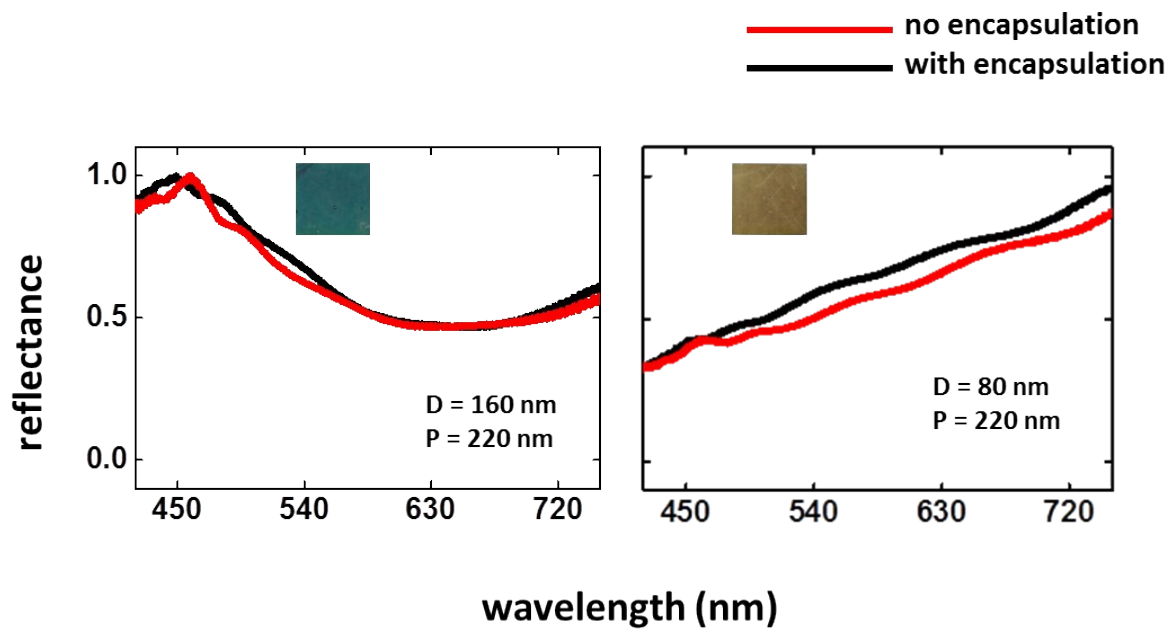


Figure S2. Measured spectra of two example structures with and without encapsulation. Encapsulation did not significantly change the perceived colors and the reflectance spectrum. The optical measurement set-up used here is same as that explained in **Figure S8g**.

S3. Comparison between constant versus varying gap configuration

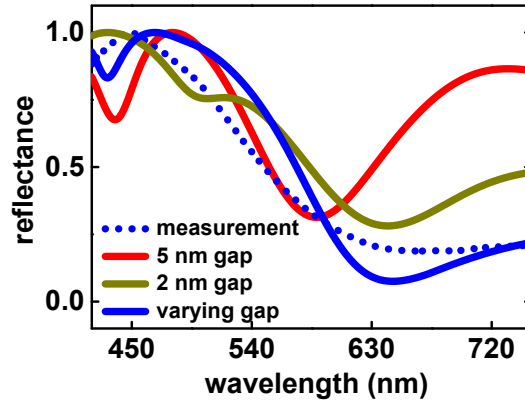


Figure S3. Simulated spectra for different constant gap sizes (2 nm and 5 nm) and the corresponding varying gap configuration for $(D,P) = (160,220)$ nm sample compared with the corresponding measured spectrum. From the figure we can see that, though the 2 nm constant gap spectrum fits better with the measured spectrum than 5 nm constant gap model, the varying gap configuration still fits the best. In reality, one cannot expect either a completely connected or completely disconnected (with constant nm sized gap) metal configuration between the Al pillar and the BR. It is by far more realistic to have connections in some regions, narrow gaps in some other regions and larger gaps in yet other regions. Hence we have used the varying gap model to represent our physical samples.

S4. Comparison of simulation spectra with sharp and rounded edges

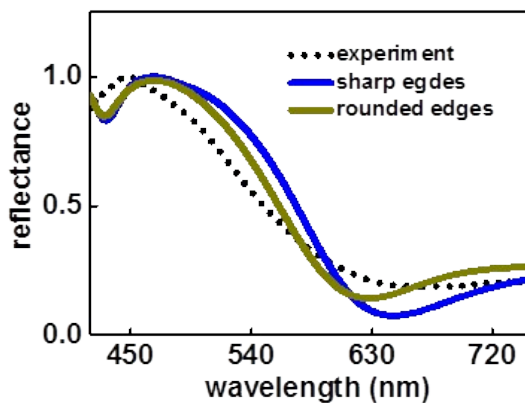


Figure S4. Simulated spectra with sharp and rounded edges compared to experiment.

S5. Coupling between pillar and cavity plasmons

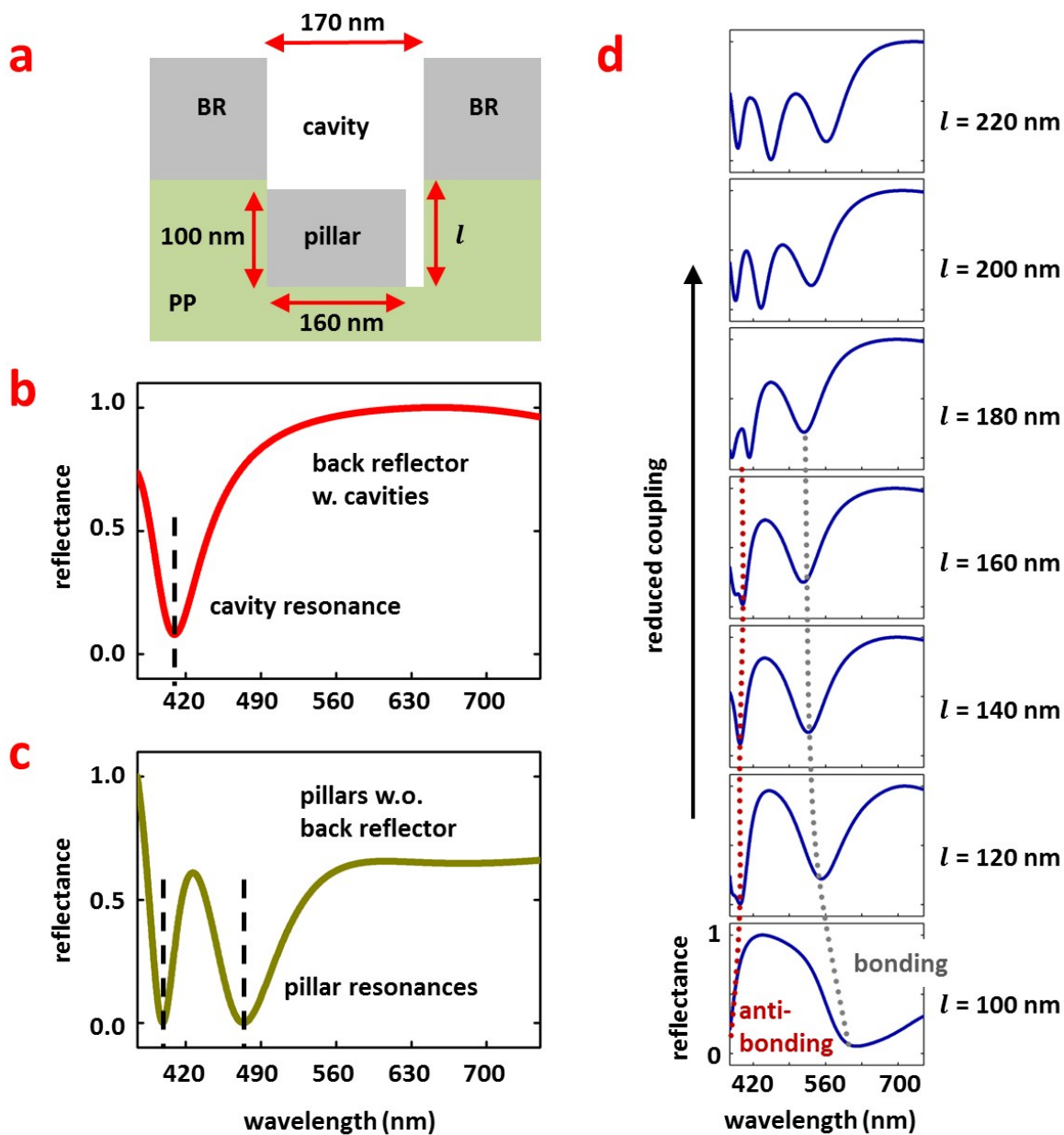


Figure S5. a: Geometry used in the simulations. Diameter of Al-pillars and metal thickness is held constant at 160 nm and 100 nm respectively, while the depth l of pits (in PP) is varied. **b:** Simulation showing the spectrum for the cavities in BR (no pillars). **c:** Simulation showing the spectrum for the Al pillars (no back reflector). **d:** Simulations showing bonding and anti-bonding modes resulting from the coupling between plasmon resonances of the pillars and cavities. As the depths of the pits (l) increase, the coupling strength reduces. At higher l , the pillar and cavity plasmons interact separately with the incident light causing respective absorption dips. The cavity plasmon interacts strongly with the high energy pillar plasmon (dip ~ 400 nm), resulting in two hybridized modes. Whereas, the interaction between the cavity plasmon and the low energy pillar plasmon (dip ~ 490 nm) has only a small influence due to large energy separation between the two modes.

S6. Diameter and depth variation at constant pitch and metal thickness

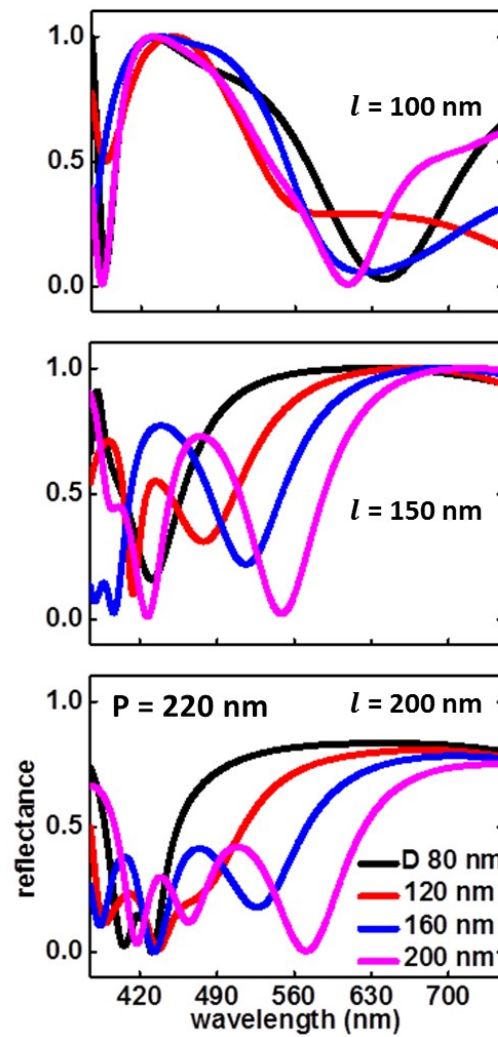


Figure S6. Simulations showing reflectance spectra for different D at pit depth of 100 nm, 150 nm and 200 nm, respectively, but constant $P = 220 \text{ nm}$ and Al thickness 100 nm.

S7. Measured and simulated spectra for 20 nm samples

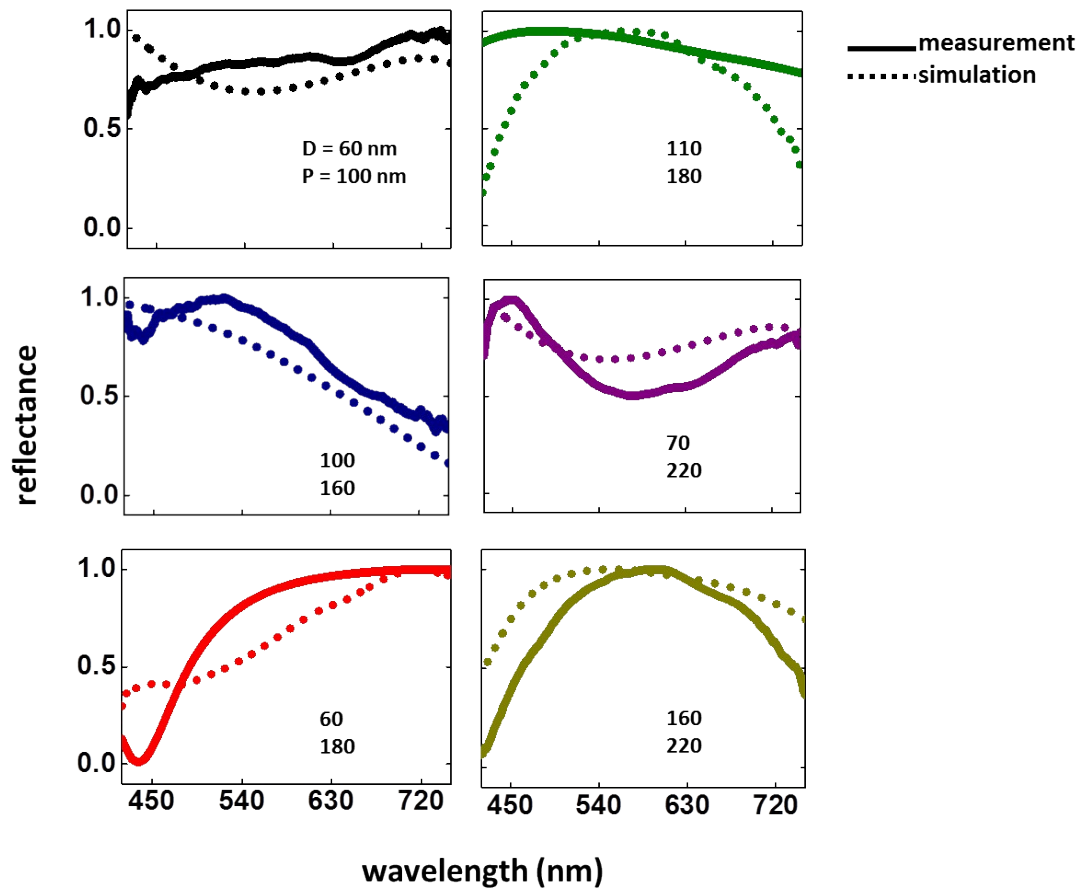


Figure S7. Simulations have been carried out for 20 nm Al samples shown in **Figure 4** and compared to the corresponding measured spectra. For the 20 nm Al samples, there could be coverage of the side walls of the nano-pits with Al (up to a certain depth) during evaporation, as shown in **Figure 4b**. We included this in the model by reducing the distance between the Al pillars and the BR to 40 nm, instead of 80 nm in an ideal scenario.

S8. Comparison of R2R and batch metalized samples

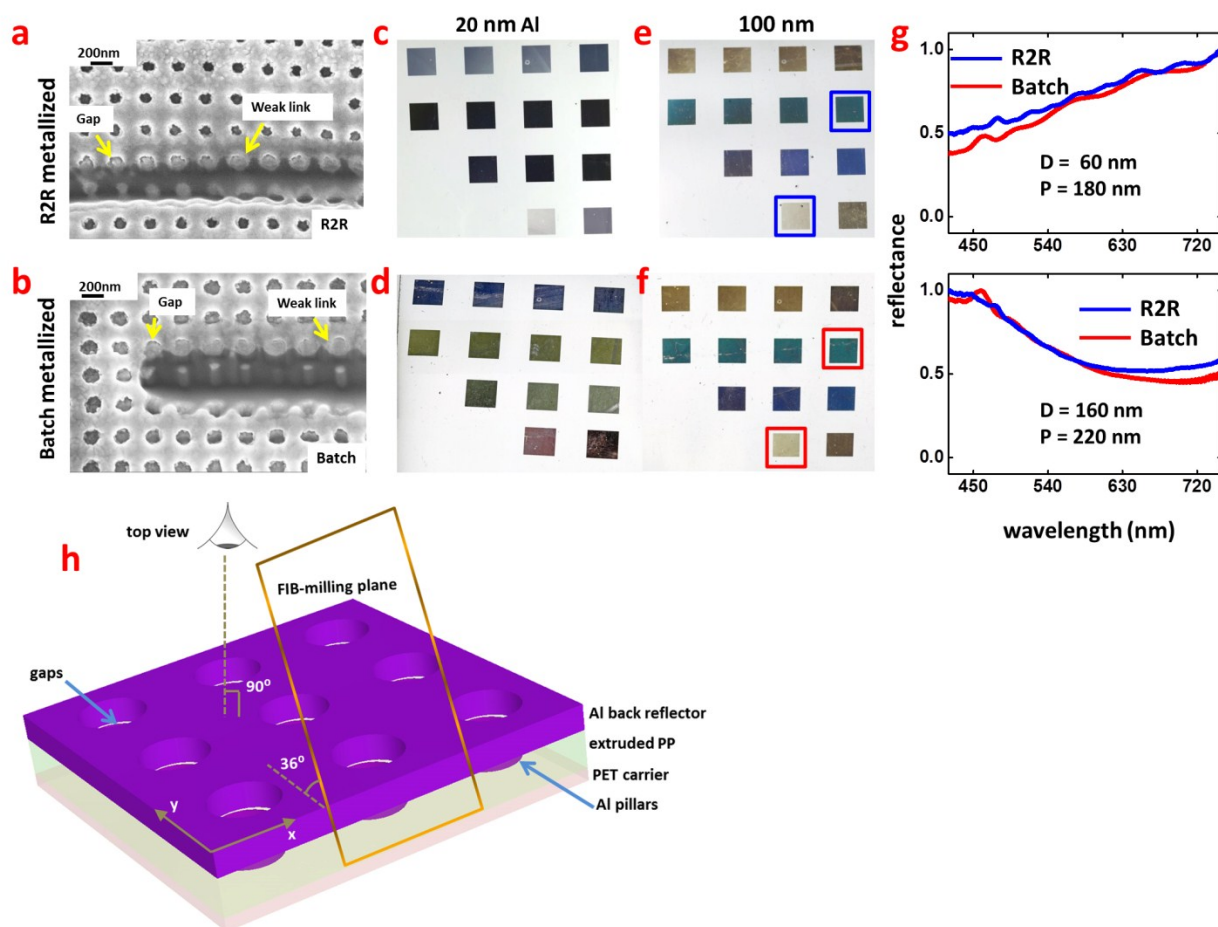


Figure S8. FIB-SEM images, **a**: R2R metalized PP foil; **b**: batch metalized PP foil. Color photographs of metalized PP foils showing that **c**: the 20 nm R2R metalized Al foil does not give the same colors as **d**: 20 nm batch metalized Al foil; whereas **e**: 100 nm R2R metalized PP foil, gives very similar colors as **f**: 100 nm batch metalized foils for the corresponding dimensions of the nanostructures. The color photographs were taken using the camera: Canon-5D-Mark-II; lens: Canon macro 100 mm. A diffused white light source (white light behind a white screen) was used for illumination. The lighting setup used was a 100 W light bulb from Bowens. **g**: Reflectance spectra for comparison of R2R metalized (blue) and batch metalized (red) representative samples (as indicated by corresponding colors in **e** and **f** samples). The spectra were obtained by illumination by a tungsten-halogen light source (Thorlabs, SLS201L), which was guided into a Navitar optical microscope (12× zoom). The microscope was equipped with an infinity-corrected objective with a magnification of 4× (Olympus, RMS4X-PF, NA = 0.13). The reflected light was then coupled to a fiber and detected by a spectrometer (Ocean Optics, USB-2000). **h**: 3D representation of the FIB-SEM imaging procedure. The FIB-milling is made over a small area at an angle of 36° to the sample surface. The SEM images are taken at 90° to the sample surface (top view). This way, we are able

to view a section of the sample sliced at 36° , instead of 90° which is used in standard FIB-SEM imaging. Hence, we reveal the metal layer at different thickness, right from the surface to the bottom of the pits in PP, as we move across the sample in Y direction.

S9. R2R metallization – principle of operation

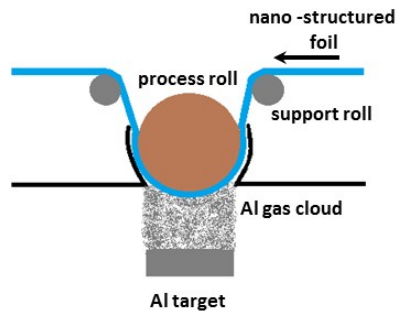


Figure S9. Schematic representation of R2R metallization (Met-Lux SA, Luxemburg). A directional Al vapor being deposited on a curved sample surface (PP foil), by thermal physical vapor deposition (PVD), at a chamber pressure of around 10^{-7} bars. The deposition angle varies between $+20^\circ$ to -20° .

S10. LED lamp spectrum

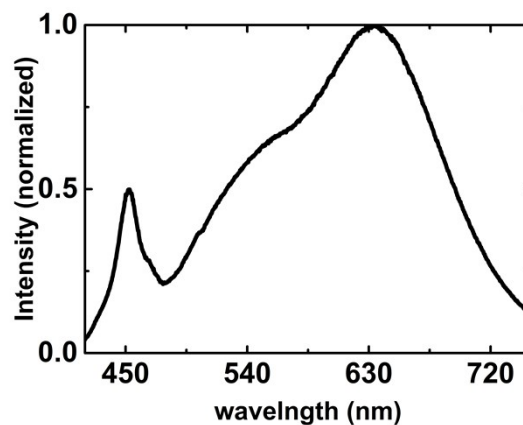


Figure S10. LED Lamp intensity spectrum – scaled to the max value.